Title

Stresses beneath dynamically applied vertical point loads

Authors

Heidarzadeh, B

Mylonakis, G

Stewart, JP

Publication Date

2023-12-10

Peer reviewed

6ICEGE 6th International Conference on Earthquake Geotechnical Engineering
1-4 November 2015
Christchurch, New Zealand

Stresses Beneath Dynamically Applied Vertical Point Loads

B. Heidarzadeh[1], G. Mylonakis [2], J. P. Stewart[3]

ABSTRACT

Engineering assessments of ground failure potential commonly express seismic demands in the form of shear stresses or normalizations thereof. In soil materials underlying foundations, referred to as 'foundation soils', dynamic stresses result from wave propagation associated with site response in combination with demands associated with soil-structure interaction (SSI). Engineers presently lack a simplified procedure for analysis of SSI-related stress demands. To provide insight into the physics of the SSI-induced stresses, and to lay the ground work for an eventual simplified procedure, this paper presents preliminary solutions for the problem of a dynamic vertical point load on the surface of an elastic half-space (Lamb's problem) and the resulting stresses within foundation soils. Results are presented in dimensionless graphical form and indicate the amplitude and phase of dynamic stresses.

Introduction

Earthquake ground shaking induces strains and stresses in soil materials as a result of wave propagation from site response. In the absence of a structure, these seismic demands on the soil materials are considered free-field. Such demands on soil materials can cause, among other effects, pore pressure generation and associated losses in shear strength and stiffness. The presence of a structure modifies the characteristics of wave propagation in the vicinity of the foundation due to soil-structure interaction (SSI); therefore, in 'foundation soils' dynamic stress demands result from both site response and SSI. In conventional engineering practice, stress demands from SSI are ignored based on the perception that demands from wave propagation are dominant. However, numerous post-earthquake field investigations [e.g., 1999 Kocaeli, Turkey (Bray and Stewart, 2000); 1999 Chi-Chi, Taiwan (Chu et al., 2004), 2011 Tohoku, Japan (Ashford et al., 2011)] provide evidence for local ground failure beneath foundations, apparently influenced by SSI-related demands. Similar phenomena have been observed and documented in centrifuge modeling (e.g., Dashti et al., 2009).

The stress solutions for static vertical and horizontal loads applied on the surface of an elastic half-space are given by exact formulae by Boussinesq (1885) and Cerruti (1882), which are available in engineering textbooks and manuals. Moreover, a few analytical and some numerical solutions exist for more general types of static loading such as circular or square vertical and horizontal loads applied on the surface of an elastic half-space or a finite soil layer over rigid rock, obtained by integration of the above solutions (Poulos & Davis 1974). In the case of dynamic loading, the body of knowledge is much more limited, primarily due to the difficulty in solving the governing differential equations in closed form. The first to successfully perform such an analysis was Lamb (1904), who extended Boussinesq's solution by considering a suddenly applied vertical load of constant amplitude. Despite several subsequent studies (summarized by Kausel 2012), little progress has occurred over the last century for two main reasons: (1) the difficulty in evaluating certain integrals (i.e., inverting

[1]Ph.D. Candidate, Dept. Civil & Environ. Eng., UCLA, Los Angeles, CA, USA, bheidarzadeh@ucla.edu
[2]Chair in Geotechnics and Soil-Structure Interaction, Univ. of Bristol, Bristol, UK, Professor, Univ. of Patras, Greece; Adjunct Professor, UCLA, Los Angeles, CA, USA, cexgm@bristol.ac.uk
[3]Professor and Chair, Dept. Civil & Environ. Eng., UCLA, Los Angeles, CA, USA, jstewart@seas.ucla.edu

the integral transforms) employed in the analysis; and (2) the focus in practice on determining surface motions, not soil stresses. An exception is a recent study by Schepers et al. (2010) on the problem of harmonic vertical and horizontal point loads on the surface of a visco-elastic half-space. However, the pressure bulbs presented are hard to use due to necessary scaling adjustments to get the corresponding stress outputs. Inspired by the aforementioned analyses, the goals of this study are to: (1) extend the Boussinesq (1885) problem to the dynamic regime, by considering a harmonic load applied on the surface of a visco-elastic half-space, (2) develop general normalization schemes to facilitate ease of application, and (3) provide insight into the physics of SSI-induced stresses and thereby take initial steps towards a simplified procedure for evaluating seismic stress demands in foundation soil.

Dimensional Analysis

The differential equations describing the response of the soil mass are not solvable analytically, so dimensional analysis is employed to capture the specific parameters that characterize the system. The Buckingham π theorem (Buckingham, 1914) is applied for static and dynamic vertical point loads applied on the surface of an elastic half-space, to determine the number of dimensionless parameters required in the solution. According to this theorem, a physical problem involving N parameters with M fundamental dimensions can be described by a set of $P = N - M$ dimensionless parameters (π groups). In other words, identifying the variables involved in a physical problem would suffice for computing the number of dimensionless parameters, even when the form of the governing equation describing the problem or the solution is unknown. It should be noted that the choice of dimensionless parameters is not specified in this theorem; therefore the process of selecting the π groups should be bounded with knowledge of physical characteristics of the corresponding problem and requires judgement.

Dimensional Analysis for the Classical Boussinesq Problem

With reference to the coordinate system of Figure 1(a), the classical Boussinesq problem is presented in Figure 1(b). In this figure the position of an arbitrary element within the elastic soil medium (with Young's modulus E and Poisson's ratio ν) is defined by radial distance R from the point of application of load P, and the vertical aperture angle, φ. Hence, in this problem, three parameters, E, R, and P have two fundamental units, i.e. length *[L]* and force *[F]*. Two intrinsically dimensionless parameters, φ and ν, complete the definition of the physical system. Accordingly, the number of dimensionless groups required to define this problem is given as (where Q refers to the number of intrinsically dimensionless parameters):

$$(N-M)+Q=(3-2)+2=3 \tag{1}$$

Therefore, the solution to the classical Boussinesq problem must be represented by an equation involving three dimensionless parameters, two of which are known (φ and ν). Additional steps are required to identify the third parameter. Equation 2 shows the stress response, σ_{ij}, of a soil element, with the associated units appearing in Equation 3.

$$\sigma_{ij} = P^{\alpha} E^{\beta} R^{\gamma} g(\varphi,\nu) \tag{2}$$

$$[\frac{F}{L^2}] = [F]^{\alpha} [\frac{F}{L^2}]^{\beta} [L]^{\gamma} \tag{3}$$

Parameters α, β, and γ are determined through dimensional analysis per Equation 3.

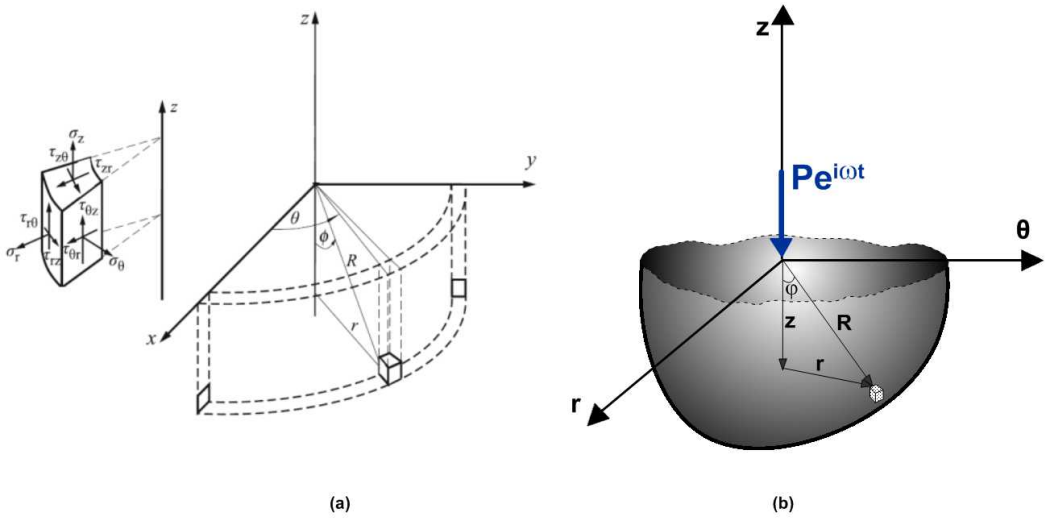

Figure 1. (a) Cartesian versus cylindrical coordinates - Adapted from Schepers et al. (2010), (b) Classical Boussinesq problem (ω = 0), Dynamic Boussinesq problem (ω > 0)

Equation 3 provides two equations and three unknowns. The linearity of the problem requires $\alpha = 1$. Values of β and γ are then obtained as 0 and -2, respectively, resulting in:

$$\sigma_{ij} = P\, g(\varphi,\nu) / R^2 \tag{4}$$

Equation 4 reveals the independence of stresses to the Young's modulus of the half-space. Equation 4 is rewritten in a dimensionless form in Equation 5 where the third dimensionless parameter is ($\sigma_{ij}R^2/P$). In other words, for an element located at distance R from the vertical static point load applied at the ground surface, the dimensionless stress depends only on aperture angle and ν. This is confirmed by the exact stress solution to the Boussinesq's problem as shown in Equations 6–9 in dimensionless forms.

$$\sigma_{ij}R^2 / P = g(\varphi,\nu) \tag{5}$$

$$\sigma_r R^2 / P = [3\cos\varphi \sin^2\varphi - (1-2\nu)/(1+\cos\varphi)] / 2\pi \tag{6}$$

$$\sigma_\theta R^2 / P = (1-2\nu)[1/(1+\cos\varphi) - \cos\varphi] / 2\pi \tag{7}$$

$$\tau_{rz} R^2 / P = 3\sin\varphi\cos^2\varphi / 2\pi \tag{8}$$

$$\sigma_z R^2 / P = 3\cos^3\varphi / 2\pi \tag{9}$$

The independence of the right-hand side of the above solutions to R indicates *self-similarity* of the problem, as it reduces the number of independent variables from two (i.e., φ, R) to one (φ), which simplifies the governing equations. This remarkable property is discussed in detail by Barenblatt (1996).

Dimensional Analysis for the Dynamic Vertical Point Load Problem

In the dynamic counterpart to the Boussinesq problem, shown in Figure 1(b), the point load is periodic with amplitude P and angular frequency ω. Radial Distance (R), shear wave velocity (V_s), shear modulus (G), and mass density of the soil medium (ρ) are other essential parameters. Since G, V_s, and ρ are correlated; only two of them should be considered as fundamental parameters resulting in a total of five (N = 5), three fundamental dimensions, length *[L]*, force *[F]*, and time *[T]*, (M = 3), and intrinsically dimensionless parameters ν, ξ, and φ (Q = 3). Accordingly, the number of dimensionless parameters is:

$$(N-M)+Q=(5-3)+3=5 \tag{10}$$

Hence, in addition to the three intrinsically dimensionless parameters and ($\sigma_{ij}R^2/P$), another dimensionless parameter is required to fully describe the dynamic solution. This parameter is selected to be ($\omega R/V_s$), which is recognized in most studies involving dynamic analysis as dimensionless frequency. A difference in the present case is that R is a coordinate, not a characteristic length (e.g. a footing dimension). Alternatively, ($\omega R/V_s$) can be interpreted as proportional to the ratio of R to wavelength. As shown in Equation 11, in the dynamic problem ($\sigma_{ij}R^2/P$) is a function of soil ν and ξ, aperture angle, and dimensionless frequency:

$$\sigma_{ij}R^2/P=g(\varphi,\nu,\xi,\omega R/V_s) \tag{11}$$

The function g in Equation 11 is not unique and changes depending on the stress component of interest. Instead of solving the governing differential equation of the system analytically, which is a formidable task, function g is investigated numerically using a Boundary Element Method implemented in the software platform ISoBEM (2012). The accuracy of ISoBEM analyses are verified for the static vertical loading problem in Figure 2, which compares vertical and shear stress results from ISoBEM analysis and the Boussinesq solution.

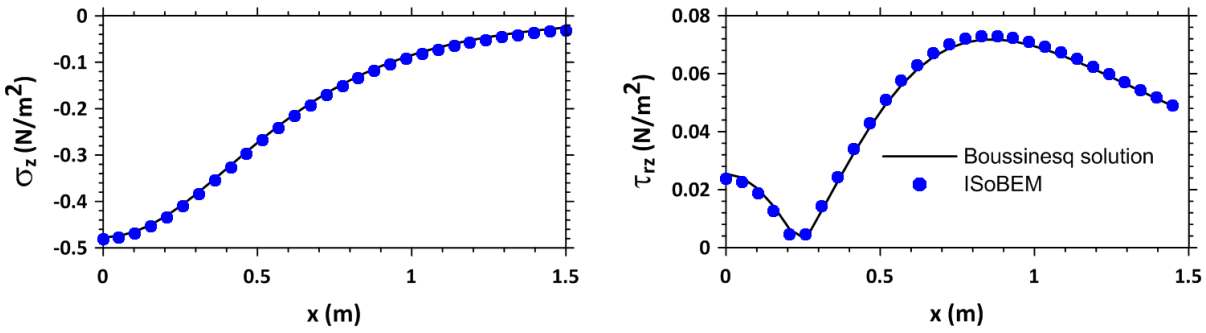

Figure 2. Comparison between ISoBEM and analytical solution for classical Boussinesq problem (y = 0, z = -1 m, P = 1 N, ρ =1.8 Mg/m^3, V_S = 100 m/s, ν = 0.33)

In the case of a harmonic vertical applied point load, a comparison is performed between vertical and shear stress results from ISoBEM analysis and the solution of Schepers et al. (2010) for ν = 0.33, ξ = 0.5%, V_S =100 m/s, and ρ =1.8 Mg/m^3. The outcomes of this comparison are presented in Table 1. The stress values corresponding to Schepers et al. (2010) were computed using a MATLAB script provided by Schepers (personal communication, 2013). While the results are generally compatible, they exhibit differences of up to approximately 25%, which is considered high for this relatively well-defined and simple problem. Accordingly, we performed additional checks of displacement results

between the MATLAB script, ISoBEM, and numerical finite element analyses performed by E. Esmaeilzadeh (personal communication, 2014) using an axisymmetric frequency domain wave solver with perfectly matched layers as absorbing boundary conditions (Esmaeilzadeh et al., 2014). Although not shown here for brevity, this comparison indicates that the results from ISoBEM analyses are generally more consistent with those from finite element simulations than with those from Schepers et al. (2010).

Table 1. ISoBEM axisymmetric verification models. SEA 2010=Schepers et al. (2010)

Freq. f (Hz)	Coords. (r,z) (m)	ISoBEM σ_z (N/m^2)	SEA 2010 σ_z (N/m^2)	σ_z Diff. (%)	Coords. (r,z) (m)	ISoBEM τ_{hv} (N/m^2)	SEA 2010 τ_{hv} (N/m^2)	τ_{hv} Diff. (%)
0	(0,-1)	0.484	0.478	1%	(0.704,-0.704)	0.170	0.170	0%
12.5	(0,-0.958)	0.595	0.468	24%	(0.758,-0.758)	0.176	0.168	5%
25	(0,-1.188)	0.530	0.462	14%	(1.032,-1.032)	0.162	0.209	25%
37.5	(0,-1.406)	0.450	0.461	2%	(1.11,-1.11)	0.177	0.166	7%
50	(0,-1.450)	0.453	0.458	1%	(1.176,-1.176)	0.144	0.114	23%

Additional verification was conducted for the normalization of the dynamic stress results with respect to ($\sigma_{ij}R^2/P$) and ($\omega R/V_s$). For this purpose, three models were built in ISoBEM representing different values of frequencies, shear wave velocities, and radial distances, yet identical sets of dimensionless frequencies, ($\omega R/V_s$). Table 2 summarizes results for the three models used for normalization verifications. Corresponding stress amplitudes are presented in Figure 3 in non-normalized and normalized forms for vertical normal stresses σ_z and in-plane shear stresses on horizontal and vertical planes τ_{hv}. The results support the proposed normalization scheme.

Table 2. ISoBEM axisymmetric models used to verify normalization; $\nu = 0.34$, $\xi = 1\%$.

	Model 1			Model 2			Model 3		
$\omega R/V_s$	ω (rad/s)	R (m)	V_s (m/s)	ω (rad/s)	R (m)	V_s (m/s)	ω (rad/s)	R (m)	V_s (m/s)
0.5	98.06	0.51	100	49.75	1.0	100	33.26	1.5	100
1	196.1	0.51	100	99.50	1.0	100	66.52	1.5	100
2	392.2	0.51	100	199.0	1.0	100	133.0	1.5	100
4	784.4	0.51	100	398.0	1.0	100	266.0	1.5	100
6	1176	0.51	100	597.0	1.0	100	399.1	1.5	100
8	1568	0.51	100	796.0	1.0	100	532.1	1.5	100
10	1961	0.51	100	995.0	1.0	100	665.1	1.5	100

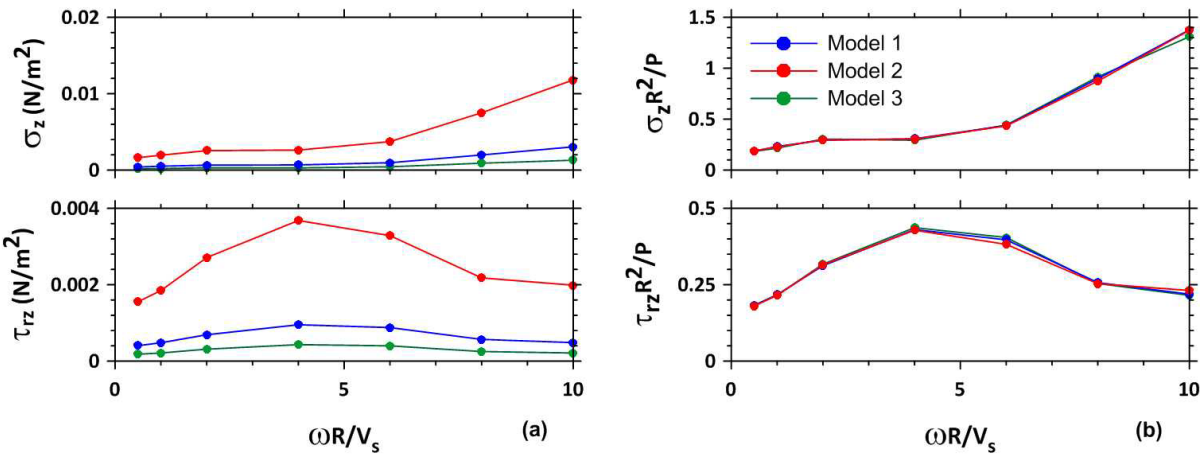

Figure 3. Checks of stress normalization using ISoBEM analyses for the conditions described in Table 2; (a) stress components (b) normalized stress components

Axisymmetric models in ISoBEM were set up to develop dimensionless graphical representations of stress fields resulting from harmonic vertical point loads on a visco-elastic half-space. The models are designed to cover the likely parameter range for practical applications. The non-zero components of dynamic stress amplitudes and phase angles are generated and plotted as polar graphs. Vertical and shear components of stress are presented in Figure 4. Stress amplitudes are found to have upper limits of about 1.0 P/R^2 for σ_z and about 1.7 P/R^2 for τ_{rz} in the examined frequency range. It is also noteworthy that the number of lobes in the stress bulbs increases with frequency, from one under static conditions to five at ($\omega R/V_S$) = 20 for σ_z, and from two in the static case to four at the highest considered dimensionless frequency for τ_{rz}. This pattern can be explained on the basis of successive zones of destructive and constructive wave interference, which is expected to become more pronounced as frequency increases.

To help interpret the results shown in Figure 4, consider the example of a point within the soil media located at r = 2.1 m and z = -2.16 m. This point is located at radial distance R = 2.5 m from the point of application of the vertical load at a vertical angle of φ = 30 degrees. If V_S = 300 m/s and ω = 60 rad/s, the dimensionless frequency is $\omega R/V_S$ = 0.5. In Figure 4, the ray along an aperture angle of 30 degrees intersects the vertical and shear stress bulbs for $\omega R/V_S$ =0.5 (i.e. solid blue curve) at dimensionless values of 0.34 and 0.19, respectively. For a unit vertical point load (P = 1 kN), vertical and shear stress amplitudes are obtained by dividing the aforementioned values by R^2 (i.e., σ_z = 54 kN/m^2 and τ_{rz} = 30 kN/m^2). The corresponding phase angles are 0.01π and 0.003π for vertical and shear components, respectively. At zero frequency (static case), the corresponding stresses are 51 and 28 kN/m^2 and the phase angles are zero.

Conclusions

The value of dimensionless stress, ($\sigma_{ij}R^2/P$), within foundation soil underlying a harmonic vertical point load at the ground surface is a function of dimensionless frequency, damping, and Poisson's ratio. The following conclusions may be drawn (emphasizing the vertical and shear components):

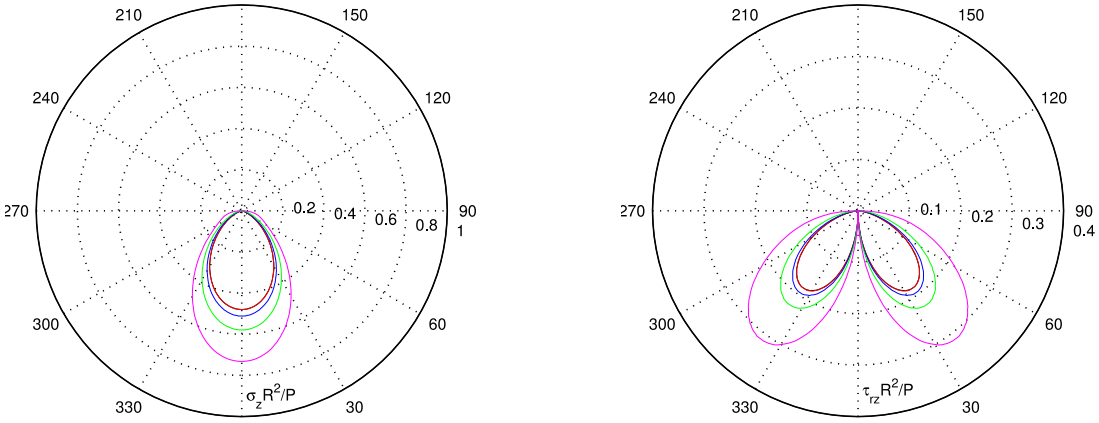

(a)

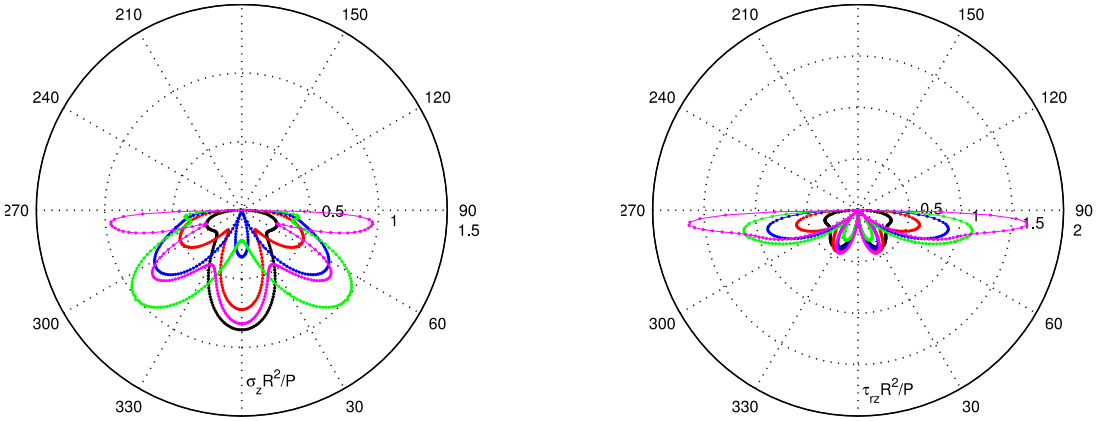

(b)

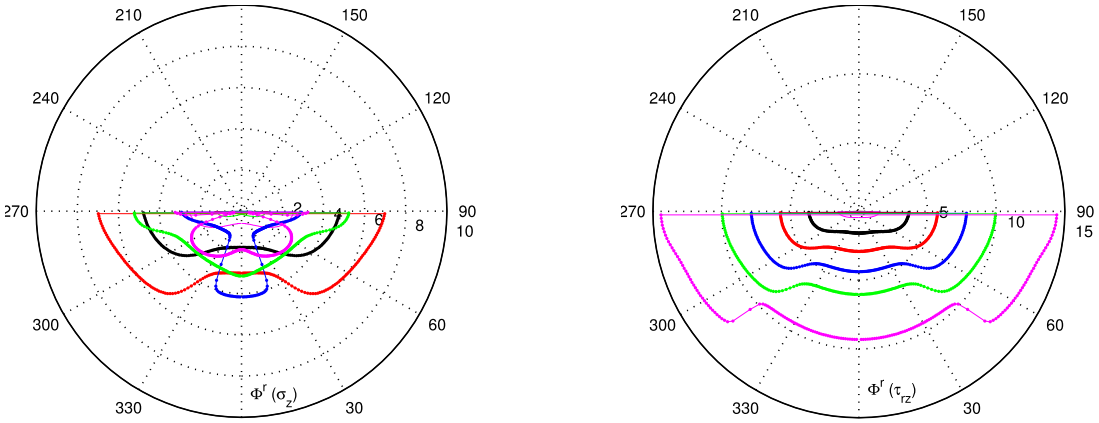

(c)

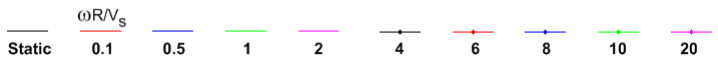

Figure 4. Stress bulbs due to vertical point load, ν = 0.34, ξ = 5%; (a) Stress amplitude bulbs for $\omega R/V_s$ = 0 (static) to 2, (b) Stress amplitude bulbs for $\omega R/V_s$ = 4 to 20, and (c) phase angle bulbs for $\omega R/V_s$ = 0 to 20.

- For ($\omega R/V_s$) < 1, dynamic effects range from negligible to moderate for both vertical and shear stress components and could probably be ignored.
- For ($\omega R/V_s$) ≈ 2 to 4, the general shapes of the stress distributions are similar to those for the static case, but the stress amplitudes are increased by about 60% for the shear component and 80% for vertical component.
- For ($\omega R/V_s$) > 4, stress patterns deviate substantially from the static case and follow a more complex pattern, due to constructive and destructive interference of the travelling waves,.
- The dynamic dimensionless stress bulbs depend on Poisson's ratio. The effects of Poisson's ratio on stress patterns (not shown here in the interest of space) and values are more significant for higher dimensionless frequencies.
- Reduction in stress values is a natural outcome of soil damping ratio. However, this effect is more obvious for higher dimensionless frequencies (also not shown in the interest of space). In other words, higher damping ratio values alleviate the dramatic sharpness in dimensionless stress bulbs with high dimensionless frequencies and cause smoother stress patterns.

When surficial loads occur across a finite area, the resulting stress distributions in the soil medium can be obtained through integration of point load solutions as presented here. This application of the present work will be presented in subsequent publications.

Acknowledgments

This research was supported in part by grant from the National Science Foundation with award number CMMI 1208170. Partial support was also provided by the UCLA Civil & Environmental Engineering Department. This support is gratefully acknowledged. The authors would like to thank Professors Dimitri Beskos and Demosthenes Polyzos of University of Patras, and Professor Stephanos Tsinopoulos of Technological Educational Institute of Patras, for providing the full version of ISoBEM and supporting the first author in the use of the software. We thank Dr. Farhang Ostadan, Professor Eduardo Kausel, and Dr. Winfried Schepers for correspondence related to this topic that advanced the work.

References

Ashford, SA, Boulanger, RW, Donahue, JL, Stewart, JP, Kokusho, T, Lee, W, Tokimatsu, K, Tsukamoto, Y, & Yoshimine, M. *Geotechnical quick report on the Kanto Plain region during the March 11, 2011, Off Pacific Coast of Tohoku earthquake, Japan.* Geotechnical Extreme Events Reconnaissance (GEER), 2011.

Barenblatt, GI. *Scaling, self-similarity, and intermediate asymptotics: dimensional analysis and intermediate asymptotics.* Vol. 14. Cambridge University Press, 1996.

Boussinesq, J. *Application des potentiels à l'étude de l'équilibre et du mouvement des solides élastiques: principalement au calcul des déformations et des pressions que produisent, dans ces solides, des efforts quelconques exercés sur une petite partie de leur surface ou de leur intérieur: mémoire suivi de notes étendues sur divers points de physique, mathematique et d'analyse.* Vol. **4**. Gauthier-Villars, 1885.

Bray, JD and Stewart, JP (principal authors). Damage patterns and foundation performance in Adapazari. *Earthquake Spectra* 2000; **16**, no. S1: 163-189.

Buckingham, E. On physically similar systems; illustrations of the use of dimensional equations. *Physical Review* **4.4** 1914; 345-376.

Cerruti, V. *Ricerche intorno all'equilibrio dei corpi elastici isotropi.* vol. 13. Rome, Italy: Reale Accademia dei Lincei, 1882.

Chu, DB, Stewart, JP, Lee, S, Tsai, JS, Lin, PS, Chu, BL, Seed, RB, Hsu, SC, Yu, MS, Wang, MCH. Documentation of soil conditions at liquefaction and non-liquefaction sites from 1999 Chi-Chi (Taiwan) earthquake. *Soil Dynamics and Earthquake Engineering* 2004; **24**, no 9-10: 647-657.

Dashti, S, Bray, JD., Pestana, JM, Riemer, M, and Wilson, D. Mechanisms of seismically induced settlement of buildings with shallow foundations on liquefiable soil. *Journal of geotechnical and geoenvironmental engineering* 2009; **136**, no. 1: 151-164.

Esmaeilzadeh Seylabi, E., Jeong, C., Taciroglu, E. (2015). On numerical computation of impedance functions for arbitrarily rigid foundations embedded in heterogeneous halfspaces, *Computers and Geotechnics*, Submitted, in review.

ISoBEM: *Boundary Element Method Package*. http://bemsands.com, 2012.

Kausel, E. Lamb's problem at its simplest. In *Proceedings of the Royal Society of London A: Mathematical, Physical and Engineering Sciences*, p. rspa20120462. The Royal Society, 2012.

Lamb, H. On the propagation of tremors over the surface of an elastic solid. *Philosophical Transactions of the Royal Society of London. Series A, Containing Papers of a Mathematical or Physical Character* 1904; 1-42.

Poulos, HG, and Davis, EH. *Elastic solutions for soil and rock mechanics.* New York: Wiley, 1974.

Schepers, W, Savidis, S and Kausel, E. Dynamic stresses in an elastic half-space. *Soil Dynamics and Earthquake Engineering* 2010; **30**, no. 9: 833-843.